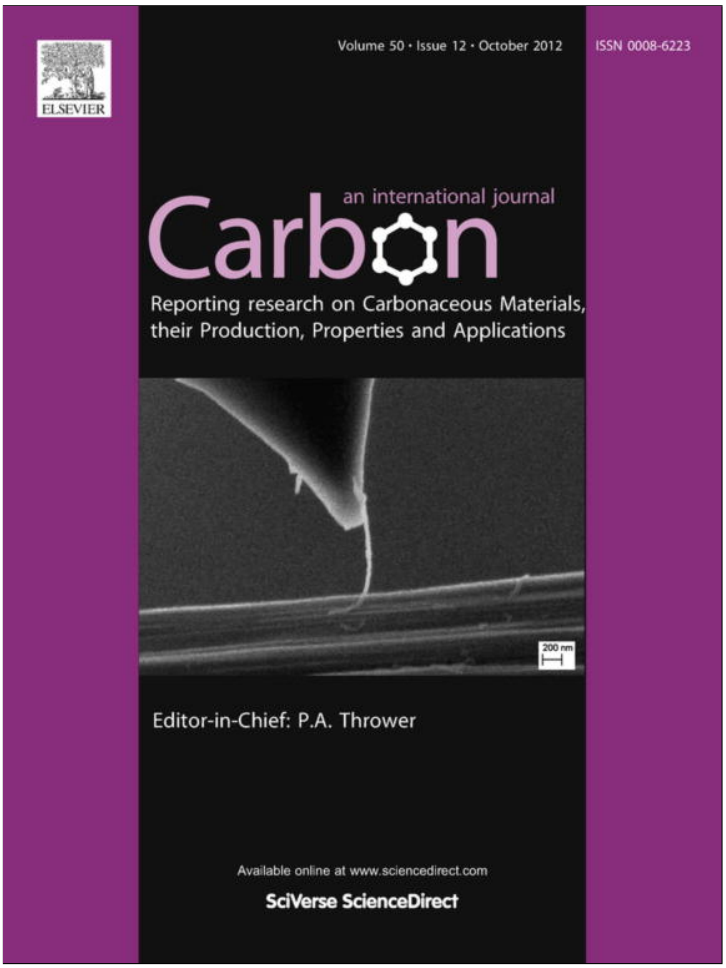

CARBON 50 (2012) 4732–4737

Available at www.sciencedirect.com

SciVerse ScienceDirect

journal homepage: www.elsevier.com/locate/carbon

Excellent field emission characteristics from few-layer graphene–carbon nanotube hybrids synthesized using radio frequency hydrogen plasma sputtering deposition

Jian-hua Deng [a], *Rui-ting Zheng* [a], *Yu-mei Yang* [a], *Yong Zhao* [b], *Guo-an Cheng* [a,*]

[a] *Key Laboratory of Beam Technology and Material Modification of the Ministry of Education, College of Nuclear Science and Technology, Beijing Normal University, Beijing 100875, China*

[b] *Department of Physics, Nanchang University, Jiangxi 330031, China*

ARTICLE INFO

Article history:
Received 20 October 2011
Accepted 27 May 2012
Available online 8 June 2012

ABSTRACT

The growth of few-layer graphene (FLG) on carbon nanotubes (CNTs) was realized by using radio frequency hydrogen plasma sputtering deposition. A defect nucleation mechanism and a two dimensional growth model of the FLG were proposed, and field emission characteristics of these FLG–CNT hybrids were studied. They show excellent field emission properties, with a low turn-on electric field (0.98 V/μm) and threshold field (1.51 V/μm), large field enhancement factor (~3980) and good stability behavior, which are much better than those of the as-grown CNT arrays. The sharp edges and the low work function of the hybrids are believed to be responsible for the improved field emission properties.

1. Introduction

Carbon nanotubes (CNTs), since they were first demonstrated as electron field emitters in 1995 [1], have been extensively studied to explore applications as electron emitting sources due to their unique structural, electrical and mechanical characteristics [2–7]. Compared with other conventional low dimensional field emission (FE) materials, such as nanofibers [8], nanorods [9], nanotips [10], and nanowalls [11], CNTs show superior FE properties, such as high emission current density (J), low turn-on electric field (E_{on}, applied field at 10 μA/cm^2) and threshold field (E_{th}, applied field at 10 mA/cm^2).

Graphene has become a rising star since its discovery in 2004 [12], and has been qualified as an attractive candidate for applications in FE sources due to its high sharp edge, incomparable electrical conductivity and excellent mechanical properties [13–16]. Graphenes can be distinguished into three types: single-, double- and few-(3–10) layer graphene (FLG) [17]. Extensive attention has been paid to FLG in the past 2 years due to its unique mechanical and electrical properties, and easy to be fabricated [18–20]. It is worth noting that the FLGs have promising FE properties due to their rich sharp edges. However, to our best knowledge, there is no report about the FE characteristics of hybrids synthesized by growing FLGs on CNT arrays forming FLG–CNT hybrids. It is worth expecting that the FLG–CNT hybrids have better FE properties, because such hybrids have advantages of the both, i.e., the high aspect ratio of CNT and the sharp edge of FLG.

In this paper, we report the uncatalyzed growth of FLG on CNT realized by radio frequency (rf) H plasma sputtering deposition. The FE characteristics of the FLG–CNT hybrids were studied. The hybrids display excellent FE properties with low E_{on} and E_{th}, large field enhancement factor and good stability, which are much better than those of the as-grown CNT arrays and other low-dimensional materials.

* *Corresponding author.* Tel./fax: +86 10 62205403.
E-mail address: gacheng@bnu.edu.cn (G.-a. Cheng).

0008-6223/$ - see front matter
http://dx.doi.org/10.1016/j.carbon.2012.05.065

2. Experimental details

2.1. FLG synthesis

Fig. 1 shows the schematic diagrams of facilities for material preparation and FE measurements. Fig. 1a shows the rf (13.56 MHz) sputtering system employed for the synthesis of FLG. The substrates used for FLG growth are CNT arrays, and the fabrication of CNT arrays has been reported previously [21]. Differing from the traditional graphene synthesis by using chemical vapor deposition (CVD) that usually involved catalyst and carbonaceous gas [22–24], the FLG growth here was catalyst-free and carbonaceous-gas-free.

Hydrogen was used not only for glow discharge but also as a sputtering gas. The sputtering target was graphite with high-purity (99.5%). The distance between the graphite target and the samples was ~6 cm. During the FLG growth, the rf power, substrate temperature, growth time, H_2 gas flow and pressure were kept at 320 W, 750 °C, 10 h, 2.5 sccm (standard cubic centimeter per minute) and 500 Pa, respectively.

2.2. Structural characterization

Morphology of the samples was characterized by scanning electron microscope (SEM, Hitachi S-4800, 10 kV) and transmission electron microscope (TEM, JEM-2010, JEOL, 200 kV). It should be emphasized that the FLG–CNT hybrids used for the SEM observation were pre-deposited an ultrathin Pt coating (~2 nm) to prevent the accumulation of static electric fields at the specimens due to the electron irradiation required during imaging. Structural information of the samples was further determined by Raman spectroscopy (LobRAM Aramis) with an excitation of 633 nm. Photoelectron spectrometer (AC-2 RIKEM KEIKI) was employed to characterize the work function of the samples.

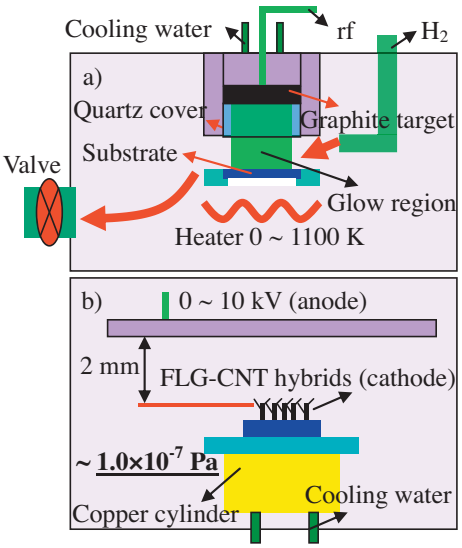

Fig. 1 – (a) Schematic diagram of the rf sputtering system utilized for FLG growth. (b) Schematic diagram of the diode configuration applied for FE measurements.

2.3. FE measurements

The FE measurements were carried out using a diode configuration in vacuum (~1.0×10^{-7} Pa) at 288 K (cooled by water), as schematically shown in Fig. 1b. The as-prepared samples were used as the cathode and a stainless steel plate was used as the anode, and the distance between the cathode and the anode was 2 mm. The emission current and applied voltage (*I*–*V*) was recorded automatically by a computer program, and the increasing rate of the applied voltage was 500 V/min.

3. Results and discussion

3.1. Structural characterization by SEM and TEM

Fig. 2a and b are low-magnification SEM images of the as-prepared CNT arrays. It can be found that the CNTs are densely packed, well aligned and having curly tips. The average length of the CNTs is about 20 μm (inset of Fig. 2a), and the diameter is around 40–60 nm. A high-resolution TEM image shown in the inset of Fig. 2b presents a typical CNT with ~60 parallel graphite layers as the tube wall. Fig. 2c and d present the side and top view of the FLG–CNT hybrids. FLGs with small sizes are sparsely distributed on the top of CNTs with sharp edges unfolded. We conjecture that the high density of the CNTs and the low carbon concentration in the sputtering system prevent the FLGs from growing in the deep CNT forest. The inconsistent sizes in the length (~300 nm) and the width (~150 nm) of the FLGs are due to the space limitation of the nano-size CNTs. The FLGs not only grow on the tips of CNTs with residual iron catalysts embedded but also on tube walls that have no catalyst left, as shown in the inset of Fig. 2c, suggesting that the secondary growth of FLG on CNT is uncatalyzed, which is quite different from the catalyzed growth of thin CNT on thick CNT reported previously [25]. The FLG displays a relatively smooth surface and a very sharp edge which is believed to act as effective field emission sites. The sharp-edge feature of the FLG can also be observed in the high resolution TEM image (inset of Fig. 2d). The FLG has 5–7 parallel graphite layers, and the layer spacing is about 0.34 nm. It should be emphasized that the layer numbers of the FLGs are ~2–10 in most cases in our study. The broken CNTs (Fig. 2c), the curled up, twisted and corrugated FLGs, and the disordered C atom arrangements (inset of Fig. 2d) suggest that structural damage has been brought into the FLG–CNT hybrids after the 10-h rf H plasma processing. However, the CNTs are still well aligned and the inner structures of the FLGs are still perfect, which is quite different from the severe structural damage induced by high-energy ion irradiating or bombarding [26]. Therefore, after a 10-h deposition, defective hybrids with sparsely distributed FLGs and well aligned CNT arrays were obtained.

3.2. Raman characterization

Raman spectrum is one of the effective methods to characterize graphene in previous researches [14,16,20,22–24,27]. In this study, Raman spectroscopy was utilized to further reveal the structural information of the products, as shown in Fig. 3.

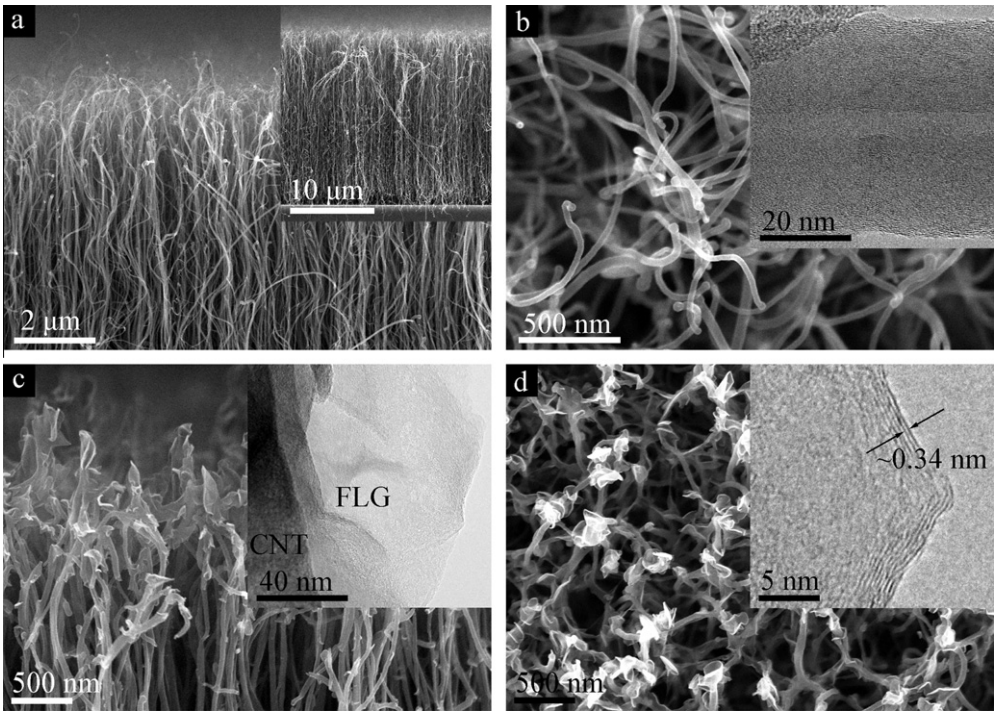

Fig. 2 – (a) SEM side view and panoramic view (inset) images of the as-grown CNT arrays. (b) SEM top view image of the as-grown CNT arrays, the inset is a high-resolution TEM image of a layered CNT. (c) SEM side view image of the FLG–CNT hybrids, the inset is a TEM image showing a hybrid structure between a CNT and a FLG. (d) SEM top view image of the FLG–CNT hybrids, the inset is a high resolution TEM image showing a curved edge of a FLG with ~5–7 graphene layers.

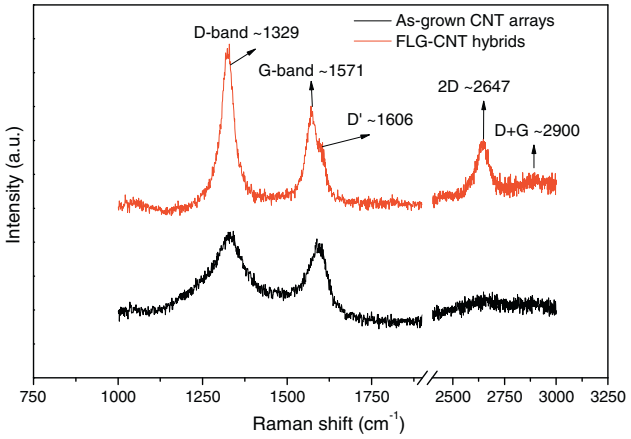

Fig. 3 – Raman spectra of the as-grown CNT arrays and the FLG–CNT hybrids.

The FLG–CNT hybrids show typical defective multilayered graphene characteristic with a sharp defect-related D peak around 1329 cm^{-1}, a broad crystalline graphite-related G peak around 1571 cm^{-1} and a broad 2D peak around 2647 cm^{-1} whose position and shape are related to the structure of graphene, especially the layer number [28–32]. The ratio of 2D peak height/G peak height is about 0.72, (~0.11 for the as grown CNT arrays), indicating the super thin feature of the FLG [28], which is consistent with our TEM observation (inset of Fig. 2d). Raman D peak reveals the disordering of the products [28–30], the intensity of which increases after the growth of FLG, indicating an increasing structure disorder. Compared to the as-grown CNTs, the Raman G peak of the hybrids broadens due to the presence of a microcrystalline-related D′ peak around 1606 cm^{-1} [28]. An unconspicuous peak at ~2900 cm^{-1} comes from the combination of the D peak and G peak [30].

3.3. *Nucleation and 2D growth model of the FLG*

We propose a two-step two dimensional (2D) growth model for the FLG, as shown in Fig. 4. The as-grown CNT arrays have

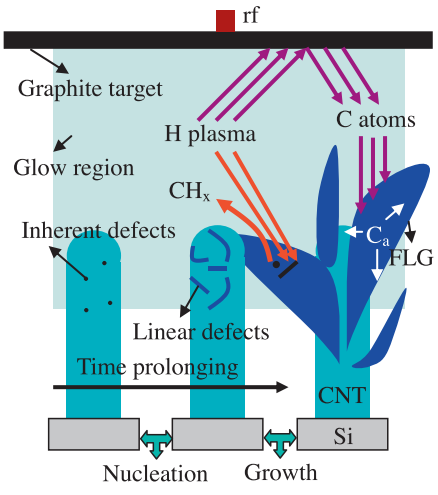

Fig. 4 – Schematic of a two-step FLG growth model: nucleation and 2D growth. C_a: activated C atoms.

inherent defects which can be observed from the TEM image (inset of Fig. 2b) and the Raman spectrum (Fig. 3). The inherent defects start to grow from point to line by absorbing sputtered activated C atoms (C_a) once the CNTs are exposed to the rf plasma. These linear defects will provide the places for the 2D FLG growth. The C_a diffusing on the surface of graphene and forming covalent bonds at the edge of graphene before being re-evaporated have been discussed previously in detail [33–35]. In brief, a long enough surface diffusion length (λ_d, the average distance that a C atom can migrate on the graphene surface before being re-evaporated) can guarantee a good running of this diffusing-bonding process so as to ensure a 2D growth of graphene. The calculated λ_d of the FLGs in our growth conditions is ~2.6 μm [33–35], which is much larger than the width (~150 nm) and the length (~300 nm) of the FLGs, that is, the 2D growth of the FLGs can advance perfectly. In addition, the etchant, hydrogen, is beneficial for promoting the crystallinity of FLG by etching away the defective C on its surface, such as forming hydrocarbon (CH_x) by chemical reaction with the defective C.

3.4. FE characteristics of the FLG–CNT hybrids

Prior to the FE measurements, an aging process was taken at ~J_{th} (threshold emission current density, 10 mA/cm^2) for 5 h to weaken influences such as absorbates induced promotion [36] and Joule heating induced degradation on FE characteristics [37]. Fig. 5 shows the plots of J as a function of E (J–E curves), and the corresponding testing results are shown in Table 1. It can be found that the E_{on} (0.98 V/μm) and E_{th} (1.51 V/μm) of the hybrids are lower than that of the as-grown CNT arrays, and it is worth nothing that they are much lower than that of the C nanofibers [8], C nanotips [10], single-layer graphene films [13], and well-aligned graphene arrays [16]. Beyond that, the largest emission current density of FLG–CNT hybrids (>70 mA/cm^2) is far larger than these 1D emitters [8,10] and pure graphene emitters [13–16]. From the differences of FE properties between the FLG–CNT hybrids and the pure graphene emitters, it is obvious that the field

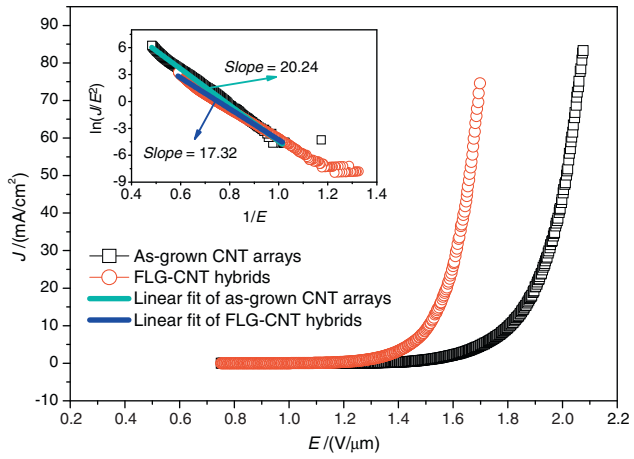

Fig. 5 – FE properties of the as-grown CNT arrays and the FLG–CNT hybrids presented in terms of J and E, and the inset is the corresponding F–N plots.

Table 1 – E_{on}, E_{th}, work function (Φ) and field enhancement factor (β) of the as-grown CNT arrays and the FLG–CNT hybrids.

Sample	E_{on} (V/μm)	E_{th} (V/μm)	Φ (eV)	β
As-grown CNT arrays	1.17	1.81	4.89	3649
FLG–CNT hybrids	0.98	1.51	4.67	3980

emission of FLGs is improved by CNT, and CNT plays a role more than a substrate.

Fowler–Nordheim (F–N) theory [38] is one of the most classical theories in the electron FE studies [1–11,13–16,21,26]. The F–N plots of ln (J/E^2) versus 1/E yield lines (inset of Fig. 5), which is in accordance with the F–N equation and indicates that the emitted electrons are extracted by the applied fields [38]. The work function (Φ) values of the as-grown CNT arrays and the FLG–CNT hybrids were obtained using photoelectron spectrometer, which are listed in Table 1 too. The decreased Φ (from 4.89 to 4.67 eV) of the FLG–CNT hybrids can be ascribed to a promotion in Fermi Level induced by the increased state density of defect after the longtime rf H plasma processing [39]. Additionally, the chemically absorbed H atoms at the dangling bonds of C can decrease the work function, either [40]. Field electron tunneling from a emission site into vacuum is determined by the local electric field (E_{loc}) at this site, E_{loc} is given by $E_{loc} = \beta E_{appl}$, where E_{appl} is the applied field and β is a geometry parameter determined by the aspect ratio of emitters, so a larger β usually means a larger local applied filed at the emission site and easier tunneling of electrons through emitters. With Φ and the constant slopes of the F–N plots, the field enhancement factor (β) of the emitters can be calculated by using the F–N equation [38], as shown in Table 1. The β of the FLG–CNT hybrids (~3980) is a little bit larger than that of the as-grown CNT arrays (~3649) but much larger than those pure graphene based emitters, such as the graphene powders [13], suggesting that the local electric fields at the emission sites of these hybrids are mainly determined by CNTs rather than graphenes themselves. Large aspect ratio (β) of CNT is the reason we choose it as the substrate for FLG growth. However, for CNT and FLG with the same length, the aspect ratio of FLG (ratio of length to thickness) is larger than that of the CNT (ratio of length to diameter), and we conjecture that this may be the main reason for the little increase of β (~331) after the growth of FLGs on CNTs. Furthermore, we must emphasize here the FLGs should be sparsely distributed on CNTs so that this field enhancement from the CNTs can not be shielded by the FLGs.

Stable field electron emission is important for practical applications. In this paper, we monitored the FE currents of the as-grown CNT arrays and the FLG–CNT hybrids at given applied fields for 20 h respectively, the results are shown in Fig. 6 and Table 2. It can be found that the applied field of the FLG–CNT hybrids at the given J_m (mean emission current density) is much lower than that of the as-grown CNT arrays whatever the J_m is around 10 or 20 mA/cm^2, which greatly facilitates practical applications. For convenience, we employ a parameter J_{drop} (J degradation during the testing time, given by $(J_{starting} - J_{last})/J_m$) to evaluate the FE stability of the

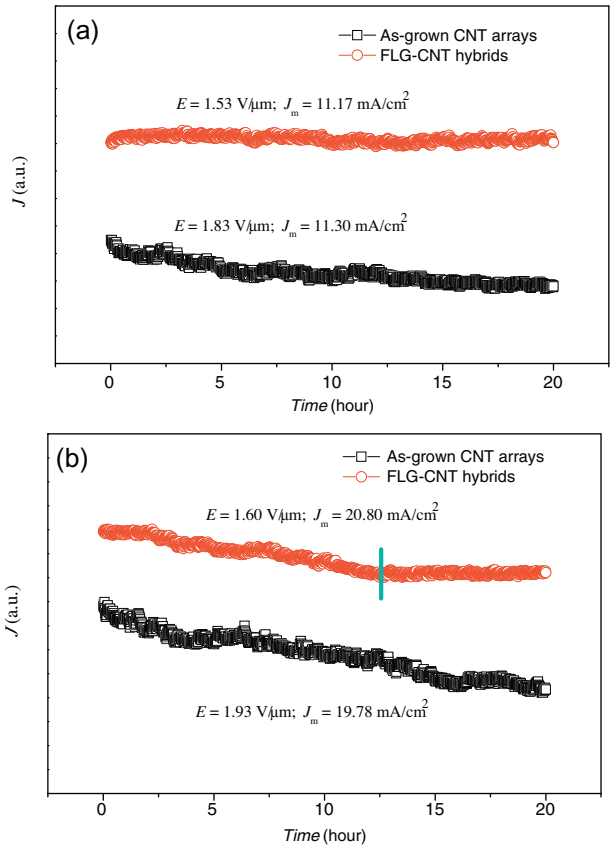

Fig. 6 – 20-h stability behavior of the as-grown CNT arrays and the FLG–CNT hybrids when J_m is around (a) 10 and (b) 20 mA/cm^2. J_m: mean emission current density.

products. When J_m is around 10 mA/cm^2 (Fig. 6a), the J_{drop} of the FLG–CNT hybrids is inappreciable (0.06%) while that of the as-grown CNT arrays is remarkable (13.45%). When the J_m is around 20 mA/cm^2 (Fig. 6b), J_{drop} of the hybrids (8.17%) is obvious, but it's still much smaller than that of the as-grown CNT arrays (15.21%). Moreover, there is an inflexion around 12.5 h in the J versus *Time* curve of the FLG–CNT hybrids (Fig. 6b, labeled by a green line). The J stops dropping and reaches a balance from the inflexion, while the J of the as-grown CNT arrays keeps dropping in the whole testing duration. CNT arrays usually have uneven surface morphologies, the protruding emitters are believed to suffer high density emission currents than others due to less field-screening [41], and those emitters are more likely to be burned off by Joule heat during FE [37]. While for planar emitters like graphene, the large-scale side length of the edge ensures a relatively uniform current distribution on its surface and greatly prevents the effective emission sites from being burned off by the Joule heat. The combination of FLG and CNT will make full use of the large aspect ratio of CNT and the stable field emission of FLG, and provide a promising candidate for FE devices.

Table 2 – Stability testing results of the as-grown CNT arrays and the FLG–CNT hybrids.

Sample	J_m (mA/cm^2)	E (V/μm)	J_{drop} (%)
As-grown CNT arrays	11.30	1.83	13.45
	19.78	1.93	15.21
FLG–CNT hybrids	11.17	1.53	0.06
	20.80	1.60	8.17

4. Summary

The growth of FLGs on CNTs was realized in an rf H plasma sputtering deposition system at 750 °C. The FLGs are sparsely distributed on the top of CNTs with 2–10 layer sharp edges. The unique structure ensures a full utilization of the advantages of CNTs (high aspect ratio) and the FLGs (rich sharp edges) during FE. The FLG–CNT hybrids present excellent FE properties, with E_{on} = 0.98 V/μm, E_{th} = 1.51 V/μm, Φ = 4.67 eV, β = ~3980, and good FE stability behavior, which are much better than that of the as-grown CNT arrays. Growth of sharp-edge FLGs on the CNTs could improve FE properties by introducing extra effective emission sites. The excellent stability behavior of the hybrids is ascribed to that the uniform current distribution on the FLG. The results suggest that FLG–CNT hybrids will be a promising candidate for the high-performance field emitters.

Acknowledgments

This work was supported by the National Basic Research Program of China (No. 2010CB832905), Fundamental Research Funds for the Central Universities, and the Program for New Century Excellent Talents in University (NCET), and partially by the National Natural Science Foundation of China (No. 11005059).

REFERENCES

[1] de Heer WA, Châtelain A, Ugarte D. A carbon nanotube field-emission electron source. Science 1995;270(5239):1179–80.
[2] Fan SS, Chapline MG, Franklin NR, Tombler TW, Cassell AM, Dai HJ. Self-oriented regular arrays of carbon nanotubes and their field emission properties. Science 1999;283(5401):512–4.
[3] Jung SM, Hahn J, Jung HY, Suh JS. Clean carbon nanotube field emitters aligned horizontally. Nano Lett 2006;6(7):1569–73.
[4] Zhu LB, Sun YY, Hess DW, Wong CP. Well-aligned open-ended carbon nanotube architectures: an approach for device assembly. Nano Lett 2006;6(2):243–7.
[5] Bonard J-M, Weiss N, Kind H, Stöckli T, Forró L, Kern K, et al. Tuning the field emission properties of patterned carbon nanotube films. Adv Mater 2001;13(3):184–8.
[6] Kim DH, Kim CD, Lee HR. Effects of the ion irradiation of screen-printed carbon nanotubes for use in field emission display applications. Carbon 2004;42(8–9):1807–12.
[7] Hojati-Talemi P, Simon GP. Enhancement of field emission of carbon nanotubes using a simple microwave plasma method. Carbon 2011;49(2):484–6.
[8] Weng CH, Leou KC, Wei HW, Juang ZY, Wei MT, Tung CH, et al. Structural transformation and field emission enhancement of carbon nanofibers by energetic argon plasma post-treatment. Appl Phys Lett 2004;85(20):4732–4.

[9] Che RC, Takeguchi M, Shimojo M, Furuya K. Field electron emission from single carbon nanorod fabricated by electron beam induced deposition. J Phys Conf Ser 2007;61(1):200–4.
[10] Tsai CL, Chen CF, Wu LK. Bias effect on the growth of carbon nanotips using microwave plasma chemical vapor deposition. Appl Phys Lett 2002;81(4):721–3.
[11] Wu YH, Yang BJ, Zong BY, Sun H, Shen ZX, Feng YP. Carbon nanowalls and related materials. J Mater Chem 2004;14(4):469–77.
[12] Novoselov KS, Geim AK, Morozov SV, Jiang D, Zhang Y, Dubonos SV, et al. Electric field effect in atomically thin carbon films. Science 2004;306(5696):666–9.
[13] Wu ZS, Pei SF, Ren WC, Tang DM, Gao LB, Liu BL, et al. Field emission of single-layer graphene films prepared by electrophoretic deposition. Adv Mater 2009;21(17):1756–60.
[14] Lahiri I, Verma VP, Choi W. An all-graphene based transparent and flexible field emission device. Carbon 2011;49(5):1614–9.
[15] Hojati-Talemi P, Simon GP. Field emission study of graphene nanowalls prepared by microwave-plasma method. Carbon 2011;49(8):2875–7.
[16] Huang CK, Ou YX, Bie YQ, Zhao Q, Yu DP. Well-aligned graphene arrays for field emission displays. Appl Phys Lett 2011;98(26):263104 (3 p.).
[17] Giem AK, Novoselov KS. The rise of graphene. Nat Mater 2007;6:183–91.
[18] Nguyen DD, Tai NH, Chueh YL, Chen SY, Chen YJ, Kuo WS, et al. Synthesis of ethanol-soluble few-layer graphene nanosheets for flexible and transparent conducting composite films. Nanotechnology 2011;22(29):295606. 8 p.
[19] Luo ZT, Somers LA, Dan YP, Ly T, Kybert NJ, Mele EJ, et al. Size-selective nanoparticle growth on few-layer graphene films. ACS Nano 2010;10(3):777–81.
[20] Zhang HX, Feng PX. Fabrication and characterization of few-layer graphene. Carbon 2010;48(2):359–64.
[21] Deng JH, Ping ZX, Zheng RT, Cheng GA. Electron transferring from titanium ion irradiated carbon nanotube arrays into vacuum under low applied fields. Nucl Instrum Methods Phys Res Sect B Beam Interact Mater Atoms 2011;269(10):1082–7.
[22] Di CA, Wei DC, Yu G, Liu YQ, Guo YL, Zhu DB. Patterned graphene as source/drain electrodes for bottom-contact organic field-effect transistors. Adv Mater 2008;20(17):3289–93.
[23] Kim KS, Zhao Y, Jang H, Lee SY, Kim JM, Kim KS, et al. Large-scale pattern growth of graphene films for stretchable transparent electrodes. Nature 2009;457:706–10.
[24] Kim UJ, Lee IH, Bae JJ, Lee S, Han GH, Chae SJ, et al. Graphene/carbon nanotube hybrid-based transparent 2D optical array. Adv Mater 2011;23(33):3809–14.
[25] Hiroyuki K, Sashiro U, Junko Y, Takeshi N, Hiromu Y, Tomotaka E, et al. Formation of secondary thin carbon nanotubes on thick ones and improvement in field-emission uniformity. Jpn J Appl Phys 2006;45(6A):5307–10.
[26] Chen KF, Deng JH, Zhao F, Cheng GA, Zheng RT. Fabricating and properties of Ag-nanoparticles embedded amorphous carbon nanowire/CNT heterostructures. Nanoscale Res Lett 2010;5(9):1449–55.
[27] Bunch JS, van der Zande AM, Verbridge SS, Frank IW, Tanenbaum DM, Parpia JM, et al. Electromechanical resonators from graphene sheets. Science 2007;315(5811):490–3.
[28] Ferrari AC, Meyer JC, Scardaci V, Casiraghi C, Lazzeri M, Mauri F, et al. Raman spectrum of graphene and graphene layers. Phys Rev Lett 2006;97(18):187401. 4 p.
[29] Tuinstra F, Koenig JL. Raman spectrum of graphite. J Chem Phys 1970;53(3):1126–30.
[30] Nemanich RJ, Solin SA. First- and second-order Raman scattering from finite-size crystals of graphite. Phys Rev B 1979;20(2):392–401.
[31] Ferrari AC, Robertson J. Interpretation of Raman spectra of disordered and amorphous carbon. Phys Rev B 2000;61(20):14095–107.
[32] Vidano RP, Fischbach DB, Willis LJ, Loehr TM. Observation of Raman band shifting with excitation wavelength for carbons and graphites. Solid State Commun 1981;39(2):341–4.
[33] Lee YH, Kim SG, Tománek D. Catalytic growth of single-wall carbon nanotubes: an Ab initio study. Phys Rev Lett 1997;78(12):2393–6.
[34] Louchev OA, Sato Y, Kanda H. Growth mechanism of carbon nanotube forests by chemical vapor deposition. Appl Phys Lett 2002;80(15):2752–4.
[35] Lewis B, Anderson JC. Nucleation and growth of thin films. London: Academic Press Inc; 1979.
[36] Maiti A, Andzelm J, Tanpipat N, von Allmen P. Effect of adsorbates on field emission from carbon nanotubes. Phys Rev Lett 2001;87(15):155502. 4 p.
[37] Dean KA, Burgin TP, Chalamala BR. Evaporation of carbon nanotubes during electron field emission. Appl Phys Lett 2001;79(12):1873–5.
[38] Fowler RH, Nordheim L. Electron emission in intense electric fields. Pro R Soc London Ser A 1928;119(781):173–81.
[39] Kim G, Jeong BW, Ihm J. Deep levels in the band gap of the carbon nanotube with vacancy-related defects. Appl Phys Lett 2006;88(19):193107. 3 p.
[40] Zhi CY, Bai XD, Wang EG. Enhanced field emission from carbon nanotubes by hydrogen plasma treatment. Appl Phys Lett 2002;81(9):1690–2.
[41] Suh JS, Jeong KS, Lee JS, Han I. Study of the field-screening effect of highly ordered carbon nanotube arrays. Appl Phys Lett 2002;80(13):2392–4.